OXFORD

Human Molecular Genetics, 2024, Vol. 33, 21, 1900–1907
https://doi.org/10.1093/hmg/ddae121
Advance access publication date 2 September 2024
Original Article

NEK1 haploinsufficiency worsens DNA damage, but not defective ciliogenesis, in *C9ORF72* patient-derived iPSC-motoneurons

Serena Santangelo[1,†], Sabrina Invernizzi[1,†], Marta Nice Sorce[2], Valeria Casiraghi[1], Silvia Peverelli[2], Alberto Brusati[3], Claudia Colombrita[2], Nicola Ticozzi[2,4], Vincenzo Silani[2,4], Patrizia Bossolasco[2], Antonia Ratti[1,2,*]

[1]Department of Medical Biotechnology and Translational Medicine, Università degli Studi di Milano, Via Fratelli Cervi 93, Segrate, Milan 20054, Italy
[2]Department of Neuroscience - Laboratory of Neuroscience, IRCCS Istituto Auxologico Italiano, Via Zucchi 18, Cusano Milanino, Milan 20095, Italy
[3]Department of Brain and Behavioral Sciences, University of Pavia, Via Bassi 21, Pavia 27100, Italy
[4]"Dino Ferrari" Center, Department of Pathophysiology and Transplantation, Università degli Studi di Milano, Via Francesco Sforza 35, Milan 20122, Italy

*Corresponding author: Department of Medical Biotechnology and Translational Medicine, Università degli Studi di Milano, Via Fratelli Cervi 93, Segrate, Milan 20054, Italy. E-mail: a.ratti@auxologico.it; antonia.ratti@unimi.it
†Co-first joint Authors.

Abstract

The hexanucleotide G_4C_2 repeat expansion (HRE) in *C9ORF72* gene is the major cause of amyotrophic lateral sclerosis (ALS) and frontotemporal dementia (FTD), leading to both loss- and gain-of-function pathomechanisms. The wide clinical heterogeneity among *C9ORF72* patients suggests potential modifying genetic and epigenetic factors. Notably, *C9ORF72* HRE often co-occurs with other rare variants in ALS/FTD-associated genes, such as *NEK1*, which encodes for a kinase involved in multiple cell pathways, including DNA damage response and ciliogenesis. In this study, we generated induced pluripotent stem cells (iPSCs) and differentiated motoneurons (iPSC-MNs) from an ALS patient carrying both *C9ORF72* HRE and a *NEK1* loss-of-function mutation to investigate the biological effect of *NEK1* haploinsufficiency on *C9ORF72* pathology in a condition of oligogenicity. Double mutant *C9ORF72/NEK1* cells showed increased pathological *C9ORF72* RNA foci in iPSCs and higher DNA damage levels in iPSC-MNs compared to single mutant *C9ORF72* cells, but no effect on DNA damage response. When we analysed the primary cilium, we observed a defective ciliogenesis in *C9ORF72* iPSC-MNs which was not worsened by *NEK1* haploinsufficiency in the double mutant iPSC-MNs. Altogether, our study shows that *NEK1* haploinsufficiency influences differently DNA damage and cilia length, potentially acting as a modifier at biological level in an *in vitro* ALS patient-derived disease model of *C9ORF72* pathology.

Keywords: ALS; *C9ORF72*; *NEK1*; iPSC-motoneurons; primary cilium

Introduction

The hexanucleotide G_4C_2 repeat expansion (HRE) in the first intron of *C9ORF72* gene represents the major genetic cause of both amyotrophic lateral sclerosis (ALS) and frontotemporal dementia (FTD) (OMIM_#105550) [1, 2]. *C9ORF72* HRE-associated pathomechanisms comprise both loss- and gain-of-function conditions, the latter characterized by the formation of toxic HRE-containing RNA foci and the translation of dipeptide-repeat proteins (DPRs) which altogether lead to alterations of several cellular pathways [3]. The wide clinical heterogeneity observed among *C9ORF72* patients, encompassing disease manifestation (ALS/FTD), age of onset, progression rate and clinical symptoms, suggests the potential influence of additional genetic and epigenetic modifying factors. Among the genetic modifiers, the oligogenicity condition in *C9ORF72* carriers has already been described, although its correlation with specific clinical features still remains uncertain [4–6]. Of note, *C9ORF72* HRE is frequently found in combination with rare variants in other ALS and/or FTD-associated genes, including *TARDBP*, *SOD1*, *FUS* and other minor genes, such as *NEK1* [7, 8]. *NEK1* heterozygous loss-of-function (LOF) variants and the missense p.Arg261His variant have been identified in about 3% of both familial and sporadic ALS cases [9, 10]. *NEK1* encodes for a serine/threonine tyrosine kinase involved in the maintenance of genomic stability and DNA damage response (DDR) [11], cell cycle regulation [12, 13], mitochondrial activity [14] and ciliogenesis [15, 16], although the biological effects of ALS-related *NEK1* mutations on these pathways remain largely unexplored.

Different studies have already used induced-pluripotent stem cells (iPSCs) and differentiated motoneurons (iPSC-MNs) to investigate the effect of *C9ORF72* HRE [17] and *NEK1* LOF mutations on DNA damage and DDR [18] and on nucleo-cytoplasmic transport [19]. However, the combined effect of distinct ALS gene variants has been poorly investigated functionally so far and patient-derived iPSC-MNs represent a suitable disease model for this purpose.

Results

Generation and characterization of iPSCs from the double mutant *C9ORF72/NEK1* ALS patient

By a genetic screening of an Italian ALS cohort (*unpublished data*) we identified a patient carrying *C9ORF72* HRE and a

Received: March 27, 2024. **Revised:** August 5, 2024

Table 1. Clinical features of the double mutant *C9ORF72/NEK1* ALS patient.

Gender	Age at onset	Site of onset	Cognitive status	Family history	Survival (months)
Female	50	Bulbar	ALSbi*	Mother with motoneuron disease, sister with multiple sclerosis	27

*ALS with behavioural impairment, based on the performance at ECAS and according to the Strong criteria [20]).

concurrent heterozygous non-sense mutation in *NEK1* gene (NEK1_NM_001199397: c.3107C > G: p.Ser1036Ter), already demonstrated to cause *NEK1* haploinsufficiency [7]. The patient showed an age of onset at 50 years, a bulbar form with progressive dysarthria, dysphagia, and gait disturbances, and behavioral impairment. Her family history revealed neurological diseases, including her mother's death from motor neuron disease and her sister with multiple sclerosis diagnosis. Segregation analysis was not possible because of the lack of genomic DNA from the other family members. The clinical features of the ALS *C9ORF72/NEK1* patient are reported in Table 1.

To investigate the impact of *NEK1* haploinsufficiency, due to the p.Ser1036Ter variant, as a possible modifying factor of *C9ORF72* pathology at biological level, we generated an *in vitro* disease model by reprogramming the primary fibroblasts of the double mutant *C9ORF72/NEK1* patient into iPSCs. The newly generated *C9ORF72/NEK1* iPSC line presented a canonical morphology (Fig. 1A) and fulfilled stemness features by expressing the typical pluripotency markers SSEA-4, alkaline phosphatase (AP) and TRA-1-60 by IF (Fig. 1B) and *SOX2*, *OCT3/4* and *NANOG* by RT-PCR (Supplementary Fig. S1A). We further assessed the pluripotency of the *C9ORF72/NEK1* iPSC line by evaluating its ability to spontaneously differentiate into the three germ layers, characterized by the expression of alpha-fetoprotein (endoderm), βIII-tubulin (ectodem) and desmin (mesoderm) markers (Supplementary Fig. S1B). The ALS double mutant iPSCs had a normal karyotype as assessed by Q-banding (Fig. 1C) and genetic analysis confirmed the presence of the HRE in *C9ORF72* gene by repeat primed-PCR (Fig. 1D) and of the heterozygous p.Ser1036Ter mutation in *NEK1* gene by Sanger sequencing (Fig. 1F). Southern blot analysis revealed HRE lengths of ~600 and ~200 units in the original patient's fibroblasts, indicating the presence of somatic mosaicism, and of ~500 units in the reprogrammed iPSC clone (Fig. 1E).

Western Blot analysis showed a significant reduction of NEK1 protein levels (0.68X) in *C9ORF72/NEK1* iPSCs compared to an iPSC line derived from a wild-type healthy individual (Fig. 1G), confirming that the *NEK1* p.Ser1036Ter mutation results in NEK1 haploinsufficiency also at protein level.

Double mutant *C9ORF72/NEK1* iPSCs show more pathological RNA foci compared to single mutant *C9ORF72* cells

To assess whether the newly generated double mutant *C9ORF72/NEK1* iPSC line maintained *C9ORF72*-associated pathological hallmarks, we analysed the presence of the RNA foci generated by the transcription of the *C9ORF72* HRE by RNA-FISH assay. For comparison of RNA foci formation we used an iPSC line we reprogrammed from an ALS patient carrying a *C9ORF72* HRE of 1100 units and the *CS52iALS-C9n1* line (Cedars-Sinai), while a wild-type healthy control iPSC line (CTR) was used as a negative control showing the complete absence of RNA foci as expected (Fig. 2A). We found that the *C9ORF72/NEK1* iPSC line had a significantly higher percentage of RNA foci-positive cells (58.6%) compared to our *C9ORF72* iPSC line (17.9%) and to *CS52iALS-C9n1* iPSCs (15.8%) (Fig. 2B). This was also associated with a higher mean number of foci per RNA-foci-positive cells (9.6 foci in *C9ORF72/NEK1* versus 1.2 foci in *C9ORF72* and 1.3 foci in CS52iALS-C9n1) (Fig. 2C).

Double mutant *C9ORF72/NEK1* iPSC-MNs show increased DNA damage levels compared to single mutant *C9ORF72* iPSC-MNs

Given previous literature data about the involvement of mutant *C9ORF72* and *NEK1* genes in the DNA damage pathway [17, 18], we analysed DNA damage response (DDR) in motoneurons (MNs) differentiated from the double mutant *C9ORF72/NEK1* patient-derived iPSC line. At day 30 of differentiation, all iPSC-MNs from *C9ORF72/NEK1*, *C9ORF72* and wild-type healthy control (CTR) lines tested positive for the expression of the neuronal markers βIII-tubulin and SMI-312 (pan-axonal neurofilaments) and of the specific motoneuronal markers choline-acetyltransferase (ChAT) (Fig. 3A) and HB9 (Supplementary Fig. S2B). No positivity was observed for GFAP by IF in our cultures, confirming the differentiation of only neuronal-motoneuronal cells (Supplementary Fig. S2B). The differentiation efficiency among the three experimental iPSC lines was assessed by gene expression analysis of βIII-tubulin and MAP2 neuronal markers and of Islet and ChAT motoneuronal markers by Q-PCR. Our data showed a similar expression of the neuronal and motoneuronal markers, with no significant differences among the iPSC-MN lines (Supplementary Fig. S2C).

To evaluate DNA damage and DDR, we induced single- and double-strand DNA breaks using the radiomimetic agent Neocarzinostatin (NCS) and investigated DNA damage levels at basal conditions, immediately after 20 min treatment with NCS and at 6 hours-rescue time point by staining for the phosphorylated form of the H2AX histone (γH2AX) (Fig. 3B), a well-established DNA damage marker, and βIII-tubulin to visualize neuronal cells (Supplementary Fig. S3). By quantifying the percentage of γH2AX foci-positive cells, we observed that all iPSC-MN lines had foci-positive cells at basal levels, with no significant differences among the experimental groups (CTR: 27.3%, *C9ORF72*: 37.0%, *C9ORF72/NEK1*: 14.0%) (Fig. 3C). After treatment with the NCS agent, the percentage of foci-positive cells significantly increased as expected in all groups (CTR: 54.3%, *C9ORF72*: 94.3%, *C9ORF72/NEK1*: 99.7%) and remained elevated at 6 hours-rescue (CTR: 54.3%, *C9ORF72*: 76.0%, *C9ORF72/NEK1*: 80.0%), without returning to the basal level values (Fig. 3C). Quantification of the mean number of γH2AX foci per foci-positive cells showed that, at basal levels, the *C9ORF72* line had a significantly higher number of foci compared to the CTR line and the *C9ORF72/NEK1* iPSC-MNs showed a significant higher number of foci compared to both *C9ORF72* and CTR iPSC-MNs (CTR: 4.1 foci, *C9ORF72*: 5.8 foci, *C9ORF72/NEK1*: 11.2 foci) (Fig. 3D). After DNA damage induction by NCS, the mean number of foci significantly increased in all groups (CTR: 9.9 foci, *C9ORF72*: 30.0 foci, *C9ORF72/NEK1*: 43.6 foci), with the double mutant line showing the greatest increase, and it then significantly decreased

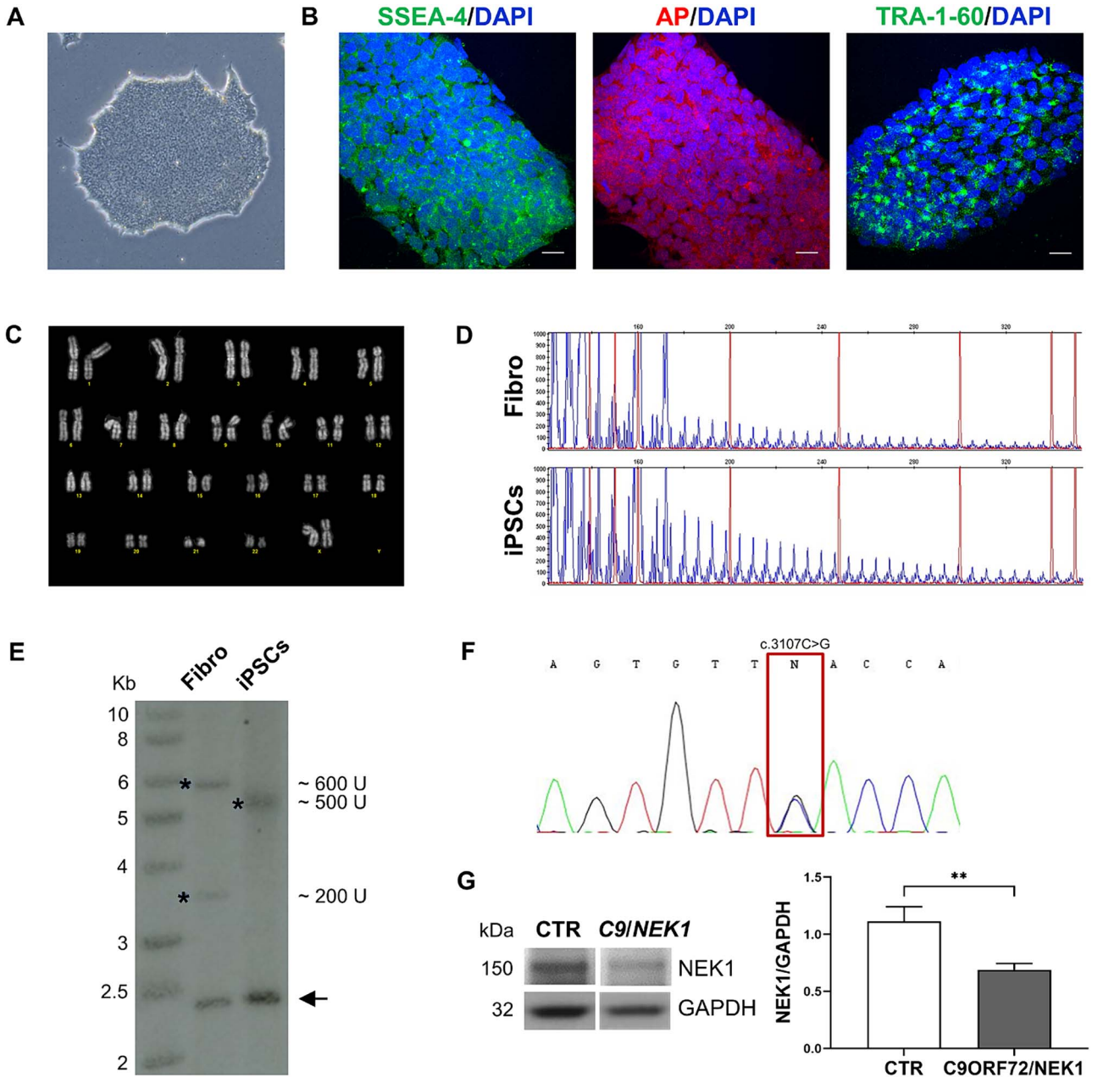

Figure 1. Characterization of the double mutant *C9ORF72/NEK1* iPSC line. (A) Representative brightfield image of a *C9ORF72/NEK1* iPSC colony. (B) Representative confocal images of pluripotency markers SSEA-4, alkaline phosphatase (AP) and TRA-1-60 in the *C9ORF72/NEK1* iPSC line; nuclei were stained with DAPI. Scale bar = 30 μm. (C) Q-banding karyotype of the *C9ORF72/NEK1* iPSC line. (D) Electropherogram of the *C9ORF72* HRE by repeat-primed PCR in *C9ORF72/NEK1* fibroblasts and iPSCs. (E) Southern blot image showing *C9ORF72* HRE in *C9ORF72/NEK1* fibroblasts and iPSCs. Asterisks indicate expanded alleles (U, units); arrows indicate the wild-type alleles. (F) Electropherogram of sanger sequencing of *NEK1* gene mutation c.3107C > G:p.Ser1036Ter in the *C9ORF72/NEK1* iPSC line. (G) Representative western blot and densitometry analysis of NEK1 protein in the wild-type healthy control (CTR) and in the *C9ORF72/NEK1* iPSC lines; all values were normalized on the CTR mean value. GAPDH was used for sample normalization. Cropped images are shown for *C9ORF72/NEK1* and CTR samples because they were originally loaded on distant lines in the same gel run. Mean ± SEM; Student's t-test (n = 3, $^{**}P < 0.01$).

at 6 hours-rescue, still maintaining the same differential pattern observed among the three experimental groups (CTR: 8.2 foci, *C9ORF72*: 12.4 foci, *C9ORF72/NEK1*: 15.0 foci).

Primary cilia are similarly defective in double *C9ORF72/NEK1* and single *C9ORF72* mutant iPSC-MNs

Since recessive *NEK1* gene mutations cause human skeletal ciliopathies [21] and NEK1 protein is involved in regulating ciliogenesis [15, 16], we decided to investigate primary cilia formation in the double mutant iPSC-MNs in comparison to *C9ORF72* and CTR iPSC-MNs. Primary cilium was visualized by IF with adenylate cyclase III (ACIII) (Fig. 4A), marker of neuronal cilia, whose signal overlaps with the other primary cilia marker Arl13b (Supplementary Fig. S4). By quantifying the percentage of cilia-positive cells, we found that both single mutant *C9ORF72* and double mutant *C9ORF72/NEK1* iPSC-MNs showed a significant decreased percentage of cilia-positive cells compared to CTR iPSC-MNs (CTR: 52.4%, *C9ORF72*: 26.7%, *C9ORF72/NEK1*: 25.9%) (Fig. 4B). Image analysis of cilium size revealed that *C9ORF72*

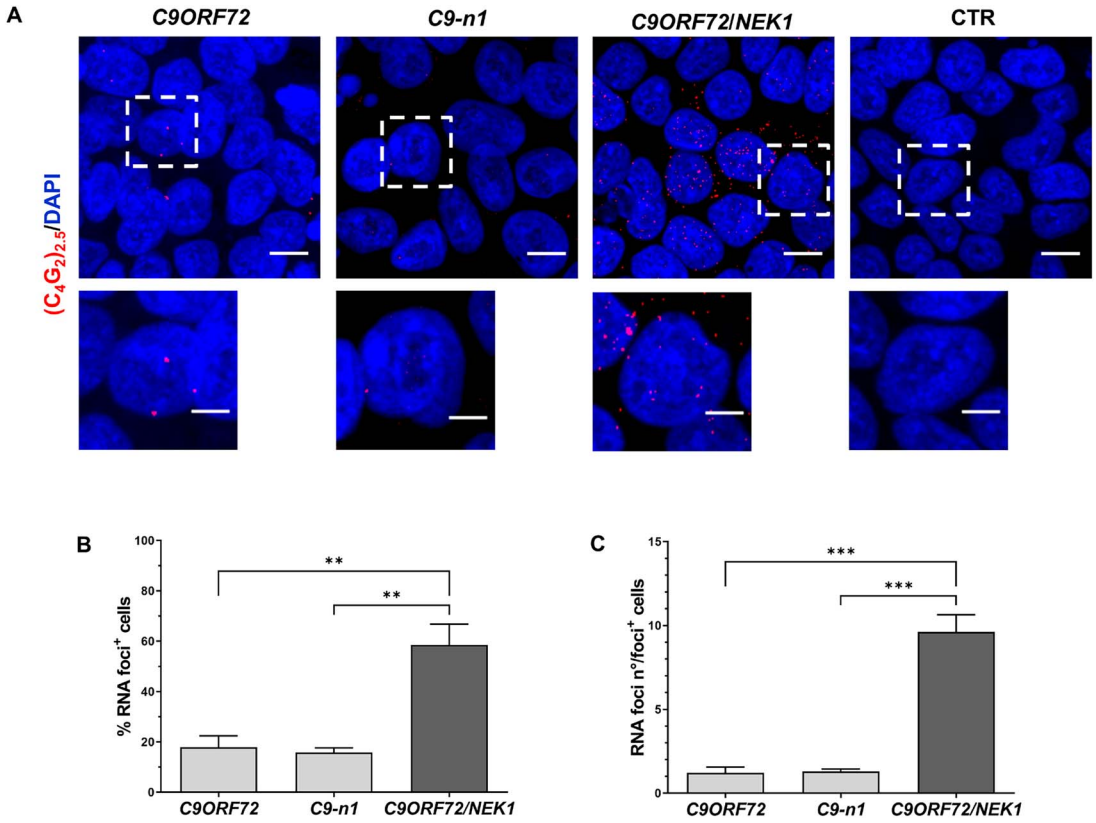

Figure 2. Analysis of *C9ORF72* RNA foci in the double mutant C9ORF72/NEK1 iPSC line. (A) Representative images of *C9ORF72* sense RNA foci in *C9ORF72*, *CS52iALS-C9n1 (C9-n1)* and *C9ORF72/NEK1* iPSC lines; nuclei were stained with DAPI. Wild-type healthy control (CTR) iPSCs were used as negative controls in FISH assay. Full image (above), scale bar = 10 μm. Inset magnification (below), scale bar = 5 μm. Quantification of (B) the percentage of *C9ORF72* RNA foci-positive cells and (C) the mean number of *C9ORF72* RNA foci per foci-positive cells in the *C9ORF72*, *C9-n1* and *C9ORF72/NEK1* iPSC lines. Mean ± SEM; Student's t-test (n = 3 at different iPSC passages in culture, > 80 cells for each replicate were analysed; *$P < 0.05$, **$P < 0.01$).

iPSC-MNs showed a significant reduced cilium length compared to CTR iPSC-MNs (CTR: 1.5 μm, *C9ORF72*: 1.0 μm) and that also *C9ORF72/NEK1* iPSC-MNs presented significantly shorter cilia (0.9 μm) (Fig. 4C). However, we found no significant differences between the single mutant *C9ORF72* and the double mutant *C9ORF72/NEK1* iPSC-MNs, neither in the percentage of cilia-positive cells (Fig. 4B), nor in the cilium length (Fig. 4C).

Discussion

In this study we analysed the biological effects of *NEK1* haploinsufficiency as a possible modifier of *C9ORF72* pathology by using *in vitro* disease models such as iPSCs obtained from an ALS patient carrying a concomitant *C9ORF72* HRE and a rare *NEK1* LOF variant. The nonsense mutation p.Ser1036Ter in *NEK1* gene has already been described to be associated to ALS aetiology in cohorts of different origins [6] and also in combination with *C9ORF72* HRE in a patient with familiar ALS, leading to a near complete loss of the mutated *NEK1* transcript, likely via nonsense-mediated mRNA decay [22]. However, there is still no functional evidence if and how this variant acts as a possible modifier on an already *C9ORF72*-mutated genetic background.

In the iPSC line generated from the double mutant ALS patient we confirmed *NEK1* haploinsufficiency, further confirming a LOF mechanism for this variant also at protein level. Interestingly, the double mutant *C9ORF72/NEK1* iPSC line showed an increased number of cells forming pathological *C9ORF72*-associated RNA foci together with a higher number of RNA foci compared to two distinct single mutant *C9ORF72* iPSC lines. There is no clear evidence in literature linking *NEK1* gene to an altered RNA metabolism that could favour the formation of pathological RNA foci. However, *NEK1* is involved in DNA damage response and *C9ORF72* RNA foci and pathological DPRs are reported to induce double strand DNA breaks and R-loops (DNA:RNA hybrids) formation [23], so that a link between pathological RNA foci transcription and NEK1 haploinsufficiency may be plausible, although still to be demonstrated mechanistically.

In line with this view, the analysis of DNA damage at baseline showed increased levels in the *C9ORF72/NEK1* double mutant cells compared to *C9ORF72* single mutant iPSC-MNs, although the response to DNA damage by NCS agent was not affected in either of the two mutant lines. However, a previous study reported defective DDR in both *C9ORF72* and *NEK1* LOF (p.Arg812Ter) single mutant iPSC-MNs [18]. This discrepancy could be due to the use of different genotoxic agents (NCS versus γ-irradiation) or to a different susceptibility of the obtained iPSC-MNs to DNA damage induction, which may also depend on the distinct protocols used to differentiate MNs in the two studies.

Of interest, we here report that the *C9ORF72* HRE affects primary cilia formation in ALS-patient derived iPSC-MNs. In neuronal cells the primary cilium acts as an antenna-like organelle responding to external stimuli and regulating several cell pathways, including autophagy [24]. Impairment of ciliogenesis and ciliary signalling has been recently associated with neurodegenerative disorders, including Parkinson's and Alzheimer's diseases [25] while, in ALS, the presence of defective cilia was described only in transgenic SOD1 mice so far [26].

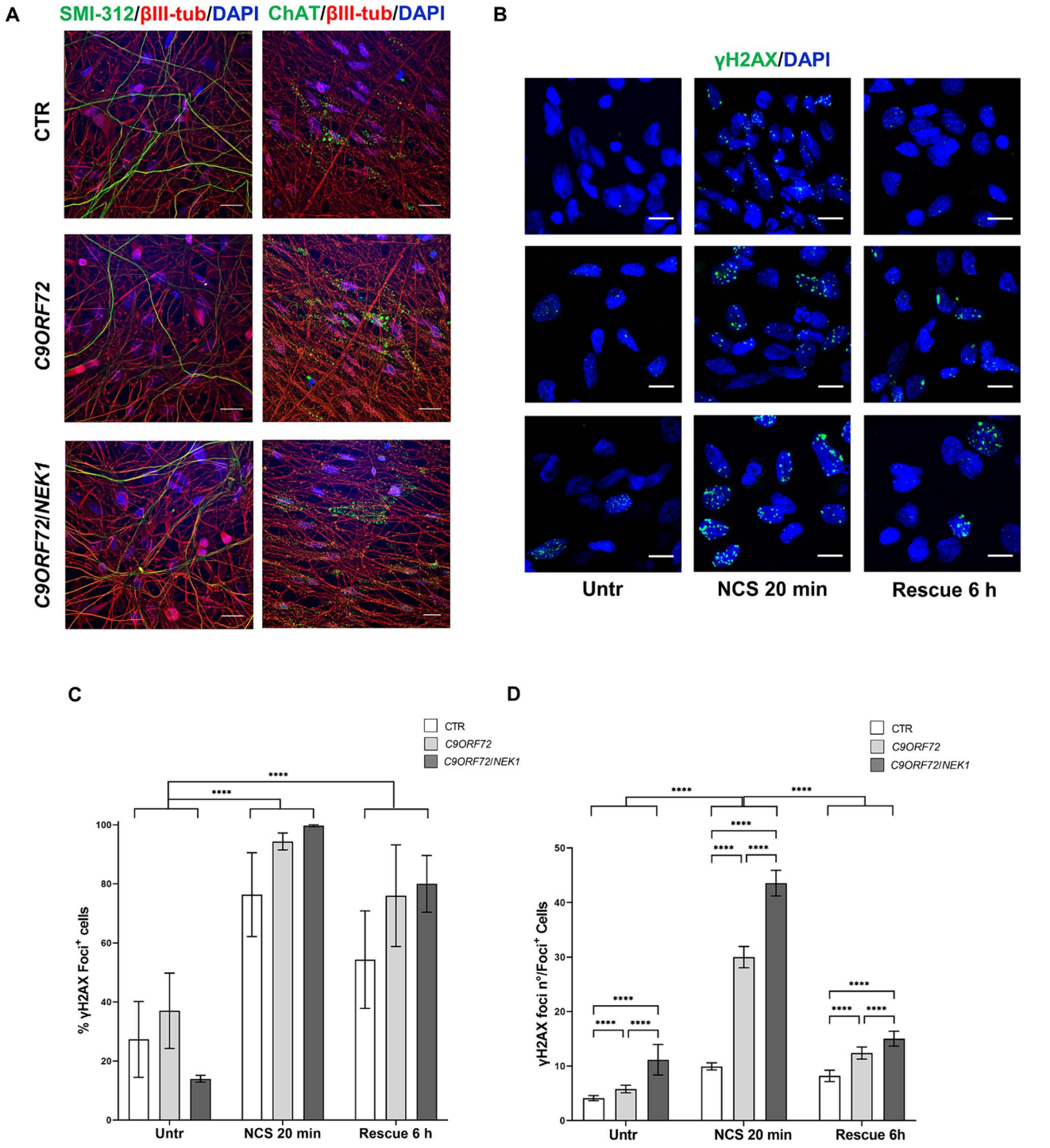

Figure 3. Analysis of DNA damage and DNA damage response (DDR) in *C9ORF72/NEK1* iPSC-MNs. (A) Representative confocal images of neuronal markers βIII-tubulin and SMI-312 and of the motoneuronal marker ChAT in wild-type healthy control (CTR), *C9ORF72* and *C9ORF72/NEK1* iPSC-derived motoneurons (iPSC-MNs); nuclei were stained with DAPI. Scale bar = 20 μm. (B) Representative confocal images of γH2AX foci in CTR, *C9ORF72* and *C9ORF72/NEK1* iPSC-MNs in untreated conditions (Untr), after Neocarzinostatin treatment for 20 min (NCS 20 min) and at 6 hours-rescue time point (rescue 6 hour); nuclei were stained with DAPI. Scale bar = 10 μm. Quantification of (C) the percentage γH2AX foci-positive cells and (D) the mean number of γH2AX foci per foci-positive cell. Mean ± SEM; two-way ANOVA, Tukey's post hoc test (n = 3 replicates of MNs differentiations, > 100 cells per condition for each replicate were analysed; ****$P < 0.0001$).

Our findings support the recent observation that C9ORF72 protein, in complex with SMCR8, acts as a major negative regulator of primary ciliogenesis [27]. Nonetheless, our data indicate that patient-derived *C9ORF72* iPSC-MNs show shorter cilium length and not longer ones, as recently described in cell lines or mice knocked-down for *C9ORF72* gene [27,28], suggesting that not only *C9ORF72* haploinsufficiency, but also RNA and DPRs gain-of-function mechanisms, may influence ciliogenesis regulation. Our results also show that the presence of an additional *NEK1* LOF mutation does not worsen *C9ORF72*

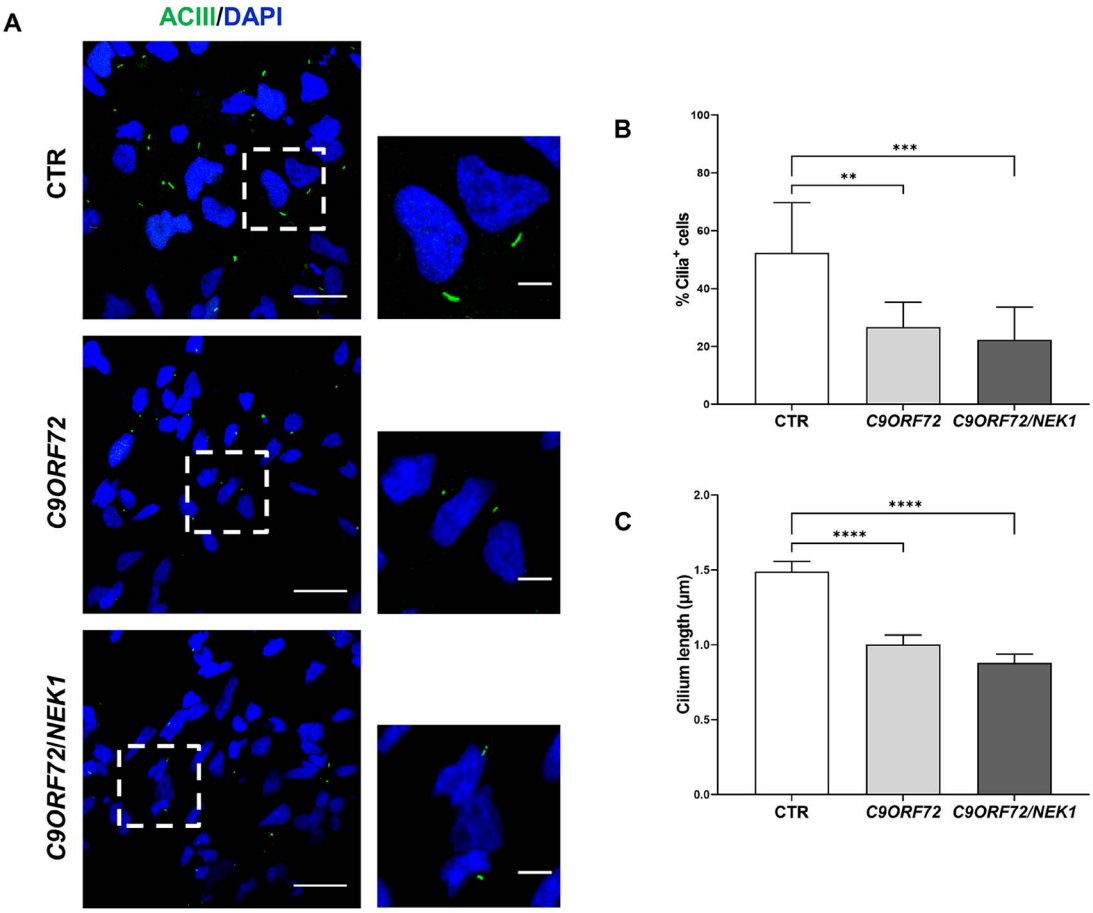

Figure 4. Analysis of primary cilia in *C9ORF72* and *C9ORF72/NEK1* iPSC-MNs. (A) Representative confocal images of primary cilium marker AC-III in wild-type healthy control (CTR), *C9ORF72* and *C9ORF72/NEK1* iPSC-motoneurons (iPSC-MNs); nuclei were stained with DAPI. Full image (left), scale bar = 10 μm; inset magnification (right), scale bar = 5 μm. Quantification of (B) the percentage of primary cilia-positive cells and (C) the mean cilium length. Mean ± SEM; one-way ANOVA, Tukey's post hoc test. (n = 3 replicates of MNs differentiations, > 200 cells for each replicate were analysed; $^{**}P < 0.01$, $^{***}P < 0.001$, $^{****}P < 0.0001$).

negative effect on primary cilia size, suggesting a not additive effect of NEK1 haploinsufficiency on ciliogenesis in contrast to what observed for DNA damage. However, preliminary data from our group report that *NEK1* haploinsufficiency alone negatively impairs ciliogenesis in iPSC-MNs and brain organoids (https://doi.org/10.1101/2024.02.29.582696), suggesting that the interplay between mutant *NEK1* and *C9ORF72* genes in DDR and ciliogenesis pathways deserves further investigation. Recently, it has been also shown that *NEK1* haploinsufficiency disrupts microtubule dynamics [19], further supporting a role of NEK1 protein in directly or indirectly regulating primary cilium length by binding to microtubules. Since NEK1 was described to regulate also nucleo-cytoplasmic transport in iPSC-MNs [19], this represents another cell pathway to be investigated in the double mutant *NEK1/C9ORF72* cells, in relationship to TDP-43 pathology.

Despite having identified a biological impact of the *NEK1* LOF mutation on different cellular pathways in patient-derived iPSC-based *C9ORF72* disease models, including increased pathological *C9ORF72* RNA foci formation and DNA damage, we did not observe any specific clinical feature which could distinguish the double mutant *C9ORF72/NEK1* ALS patient from those harbouring only *C9ORF72* HRE. This certainly sustains that ALS disease aetiology is very complex also in familial or mutation-associated cases with a variety of still-to-be-identified modifiers, including additional genetic risk factors and epigenetic modifications, which may determine the final clinical outcome and account for the vast heterogeneity observed among ALS patients. Nevertheless, our study supports the use of patient-derived iPSCs as suitable *in vitro* disease models to investigate the contribution of multiple genetic variants as possible modifying factors in *C9ORF72*-associated pathology with the aim to functionally assess their biological relevance in the context of an oligogenic condition.

Materials and methods

iPSC reprogramming and culturing

Primary fibroblasts of the double mutant *C9ORF72/NEK1* patient were isolated from skin biopsy as previously described [29] after written informed consent and approval by the ethics committee (2015-03-31-07). iPSC reprogramming was performed using the CytoTune®-iPS 2.0 Sendai Reprogramming Kit (*Thermo Fisher Scientific*) as previously described [30]. The obtained iPSC clones were cultured in E8 medium (*Thermo Fisher Scientific*) and passaged twice a week using 0.5 mM PBS/EDTA.

Spontaneous differentiation assay was performed as previously described [31]. Briefly, iPSCs were grown in suspension for 7 days to generate embryoid bodies (EBs) and they were then plated on Matrigel-coated (Corning) coverslips and grown in E8 medium for additional 10 days. iPSC lines derived from a wild-type healthy individual [32] and a mutant *C9ORF72* patient were

previously generated and characterized as described [30]. The CS52iALS-C9n1 iPSC line was obtained by Cedars-Sinai.

iPSC-MNs differentiation and DNA damage induction

iPSCs were grown in suspension for 21 days to generate EBs, that were then dissociated and cultured for additional 30 days to obtain iPSC-MNs, as previously described [30]. DNA damage was induced with 20 μM Neocarzinostatin (NCS) (*Merck*) for 20 min [33] with a subsequent 6-hours rescue timeframe from NCS treatment.

Genetic analyses

Genomic DNA was extracted from fibroblasts and iPSCs using the Wizard® Genomic DNA Purification Kit (*Promega*). *C9ORF72* HRE was tested by repeat-primed PCR (RP-PCR) as previously described [34]. To determine HRE size, Southern Blot analysis was performed using a ^{32}P-radioactive probe recognizing a unique region flanking the *C9ORF72* repeat sequence, as previously reported [34]. The heterozygous *NEK1* nonsense mutation p.Ser1036Ter was assessed by Sanger sequencing using specific primers (FOR_TATTTTCCTGATATGTGGGTTTT and REV_TGGATGTGTGTTTGTGTCTGT) and the amplicon was sequenced on an ABI 3500 Genetic Analyzer (*Applied Biosystems*). Q-banding was used for cytogenetic analysis of the iPSC line as already described [31].

Gene expression analyses

Total RNA was extracted from iPSCs using Trizol Reagent (*Thermo Fisher Scientific*) following manufacturer's instruction and reverse transcribed using SuperScript II reverse transcriptase (*Thermo Fisher scientific*) and oligo-dT primers. RT-PCR was performed using the primers pairs for the stemness markers *SOX2, OCT3/4 and NANOG* as already reported [30]. Amplicons were resolved on 2% agarose gels.

Quantitative-PCR (Q-PCR) was performed with SYBR Green PCR Master mix (*Thermo Fisher Scientific*) and 300 nM of specific primer pairs for 45 cycles on QuantStudio 12 K Flex system (*Applied Biosystems*) in duplicates. The mean Ct value of the housekeeping gene *RPL10* was used for normalization of each target gene. Each ΔCt of the experimental samples was then normalized over the mean ΔCt of the control sample ($\Delta\Delta$Ct). Gene expression values were expressed as fold change ($2^{-\Delta\Delta Ct}$).

All primer sequences used for RT-PCR and Q-PCR are listed in Supplementary Table S1.

Western blot

Cell pellets were incubated in lysis buffer (20 mM Tris–HCl pH 7.5, 150 mM NaCl, 1 mM EDTA, 1 mM EGTA, 1% Triton X-100, protease inhibitor cocktail (*Roche*)), sonicated and centrifuged at 13 000 × *g* at 4°C for 15 min. Protein extracts were quantified using the Pierce™ BCA Protein Assay Kit (*Thermo Fisher Scientific*) and 40 μg of protein lysates were resolved on precast 3%–8% gels in Tris-acetate buffer and then transferred to nitrocellulose membranes (all from *Thermo Fisher Scientific*). Membranes were blocked with 5% (w/v) non-fat dry milk in Tris-buffered saline (*Santa Cruz Biotechnology*) with Tween-20 (*Sigma-Aldrich*) (TBST) buffer and incubated with primary antibodies (Supplementary Table S2) in blocking solution at 4°C overnight and with HRP-conjugated secondary antibodies (Supplementary Table S2) for 1 hour at room temperature. The Clarity™ Western ECL Substrate (*Biorad*) was used for signal detection and densitometric analyses were performed using the Quantity One software (*Biorad*).

Immunofluorescence

Immunofluorescence (IF) was performed as previously described [35]. Briefly, cells were fixed in 4% paraformaldehyde (*Santa Cruz Biotechnology*) for 20 min and permeabilized with ice-cold methanol and with 0.3% Triton X-100 for 5 min each. Blocking was performed in 10% Normal Goat Serum (*Gibco*) in PBS for 20 min at room temperature and cells were incubated with primary antibodies (Supplementary Table S2) at 37°C for 1.5 hour and then with secondary antibodies (Supplementary Table S2) for 45 min in blocking solution at room temperature. Nuclei were stained with 4′6-diamidino-2-phenylindole (DAPI) (*Merck*).

RNA-fluorescence In situ hybridization

RNA-Fluorescence In Situ Hybridization (RNA-FISH) was performed as previously described [30]. Briefly, fixed cells in 4% paraformaldehyde were permeabilized with 0.2% Triton X-100 for 10 min and dehydrated with 70%, 90%, 100% ethanol for 5 min each in a desiccant chamber. Pre-hybridization was performed in 50% formamide (*IBI Scientific*), 50 mM sodium phosphate, 10% dextran sulphate (*Merck*) and 2X saline-sodium citrate (SSC) at 66°C for 1 hour. Hybridization was performed at 66°C overnight with 40 nM 5′TYE-563-labelled locked nucleic acid (LNA)-$(C_4G_2)_{2.5}$ probe (*Exiqon Qiagen*). Cells were then washed once in 2X SSC/0.1% Tween-20 for 5 min and three times in 0.1X SSC for 10 min at RT before being dehydrated as above and nuclei stained with DAPI.

Image acquisition and analyses

Images were acquired using the confocal Eclipse Ti microscope (*Nikon*) as Z-stacks (0.5 μm step size for IF images, 0.2 μm step size for RNA-FISH images) at 60X magnification. Images were analysed with the *ImageJ* software (https://imagej.nih.gov/ij). In particular, for quantitative analysis of *C9ORF72* RNA foci and γH2AX foci, the "Find Maxima" function and the CiliaQ plugin [36] were used, respectively, after setting an appropriate threshold, that was maintained equal for all the three experimental replicates. The percentage of yH2AX/cilia-positive cells was determined by evaluating the number of cells that showed at least one focium/cilium per cell according to the *ImageJ* software analysis.

Statistical analysis

Statistical analyses were conducted using the Graphpad Prism 9 software, using Student's t-test, one-way ANOVA or two-way ANOVA with Tukey's multiple comparison *post hoc* test. Results were considered statistically significant if $P \leq 0.05$. Bar charts represent the mean ± standard error mean (SEM).

Acknowledgements

SS, SI and VC were recipients of fellowships from the PhD program in 'Experimental Medicine', Università degli Studi di Milano. The authors acknowledge Dr Claudia Fallini (University of Rhode Island, USA) and Dr Sofia Francia (IGM-CNR, Italy) for their helpful suggestions and Dr Jan Hensen (University of Bonn, Germany) for his help with the CiliaQ plugin.
AR acknowledges 'Aldo Ravelli Center for Neurotechnology and Experimental Brain Therapeutics', Università degli Studi di Milano; VS acknowledges the ERN Euro-NMD.

Supplementary data

Supplementary data is available at *HMG Journal* online.

Conflict of interest statement: The authors declare no competing interests.

Funding

The publication fee has been supported by BIBLIOSAN - The project has been supported by the Grant [GR-2016-02364373] from the Italian Ministery of Health. NT received financial support from PSR 2021 grant, Università degli Studi di Milano.

Data availability

Experimental raw data are available on Zenodo (DOI 10.5281/zenodo.10650632).

References

1. Renton AE, Majounie E, Waite A. *et al.* A Hexanucleotide repeat expansion in C9ORF72 is the cause of chromosome 9p21-linked ALS-FTD. *Neuron* 2011;**72**:257–268.
2. DeJesus-Hernandez M, Mackenzie IR, Boeve BF. *et al.* Expanded GGGGCC Hexanucleotide repeat in noncoding region of C9ORF72 causes chromosome 9p-linked FTD and ALS. *Neuron* 2011;**72**:245–256.
3. Balendra R, Isaacs AM. C9orf72-mediated ALS and FTD: multiple pathways to disease. *Nat Rev Neurol* 2018;**14**:544–558.
4. Ross JP, Leblond CS, Laurent SB. *et al.* Oligogenicity, C9orf72 expansion, and variant severity in ALS. *Neurogenetics* 2020;**21**: 227–242.
5. Van Daele SH, Moisse M, van Vugt JJFA. *et al.* Genetic variability in sporadic amyotrophic lateral sclerosis. *Brain* 2023;**146**: 3760–3769.
6. Ruf WP, Boros M, Freischmidt A. *et al.* Spectrum and frequency of genetic variants in sporadic amyotrophic lateral sclerosis. *Brain Commun* 2023;**5**:fcad152.
7. Nguyen HP, Van Broeckhoven C, van der Zee J. ALS genes in the genomic era and their implications for FTD. *Trends Genet* 2018;**34**: 404–423.
8. Riva N, Pozzi L, Russo T. *et al.* NEK1 variants in a cohort of Italian patients with amyotrophic lateral sclerosis. *Front Neurosci* 2022;**16**:833051.
9. Brenner D, Müller K, Wieland T. *et al. NEK1* mutations in familial amyotrophic lateral sclerosis. *Brain* 2016;**139**:e28–e28.
10. Kenna KP, van Doormaal PTC, Dekker AM. *et al.* NEK1 variants confer susceptibility to amyotrophic lateral sclerosis. *Nat Genet* 2016;**48**:1037–1042.
11. Chen Y, Chen C-F, Riley DJ. *et al.* Nek1 kinase functions in DNA damage response and checkpoint control through a pathway independent of ATM and ATR. *Cell Cycle* 2011;**10**: 655–663.
12. Chen Y, Chen P-L, Chen C-F. *et al.* Never-in-mitosis related kinase 1 functions in DNA damage response and checkpoint control. *Cell Cycle* 2008;**7**:3194–3201.
13. Pelegrini AL, Moura DJ, Brenner BL. *et al.* Nek1 silencing slows down DNA repair and blocks DNA damage-induced cell cycle arrest. *Mutagenesis* 2010;**25**:447–454.
14. Martins MB, Perez AM, Bohr VA. *et al.* NEK1 deficiency affects mitochondrial functions and the transcriptome of key DNA repair pathways. *Mutagenesis* 2021;**36**:223–236.
15. Shalom O, Shalva N, Altschuler Y. *et al.* The mammalian Nek1 kinase is involved in primary cilium formation. *FEBS Lett* 2008;**582**:1465–1470.
16. White MC, Quarmby LM. The NIMA-family kinase, Nek1 affects the stability of centrosomes and ciliogenesis. *BMC Cell Biol* 2008;**9**:29.
17. Lopez-Gonzalez R, Lu Y, Gendron TF. *et al.* Poly(GR) in C9ORF72 -related ALS/FTD compromises mitochondrial function and increases oxidative stress and DNA damage in iPSC-derived motor neurons. *Neuron* 2016;**92**:383–391.
18. Higelin J, Catanese A, Semelink-Sedlacek LL. *et al.* NEK1 loss-of-function mutation induces DNA damage accumulation in ALS patient-derived motoneurons. *Stem Cell Res* 2018;**30**:150–162.
19. Mann JR, McKenna ED, Mawrie D. *et al.* Loss of function of the ALS-associated NEK1 kinase disrupts microtubule homeostasis and nuclear import. *Sci Adv* 2023;**9**:eadi5548.
20. Strong MJ, Abrahams S, Goldstein LH. *et al.* Amyotrophic lateral sclerosis - frontotemporal spectrum disorder (ALS-FTSD): revised diagnostic criteria. *Amyotroph Lateral Scler Frontotemporal Degener* 2017;**18**:153–174.
21. Thiel C, Kessler K, Giessl A. *et al.* NEK1 mutations cause short-rib polydactyly syndrome type Majewski. *Am J Hum Genet* 2011;**88**: 106–114.
22. Nguyen HP, Van Mossevelde S, Dillen L. *et al.* NEK1 genetic variability in a Belgian cohort of ALS and ALS-FTD patients. *Neurobiol Aging* 2018;**61**:255.e1–255.e7.
23. Walker C, Herranz-Martin S, Karyka E. *et al.* C9orf72 expansion disrupts ATM-mediated chromosomal break repair. *Nat Neurosci* 2017;**20**:1225–1235.
24. Mill P, Christensen ST, Pedersen LB. Primary cilia as dynamic and diverse signalling hubs in development and disease. *Nat Rev Genet* 2023;**24**:421–441.
25. Ma R, Kutchy NA, Chen L. *et al.* Primary cilia and ciliary signaling pathways in aging and age-related brain disorders. *Neurobiol Dis* 2022;**163**:105607.
26. Ma X, Peterson R, Turnbull J. Adenylyl cyclase type 3, a marker of primary cilia, is reduced in primary cell culture and in lumbar spinal cord in situ in G93A SOD1 mice. *BMC Neurosci* 2011;**12**:71.
27. Tang D, Zheng K, Zhu J. *et al.* ALS-linked C9orf72–SMCR8 complex is a negative regulator of primary ciliogenesis. *PNAS* 2023;**120**:e2220496120.
28. Tang D, Bao H, Qi S. The C9orf72-SMCR8 complex suppresses primary ciliogenesis as a RAB8A GAP. *Autophagy* 2024;**20**: 1205–1207.
29. Onesto E, Colombrita C, Gumina V. *et al.* Gene-specific mitochondria dysfunctions in human TARDBP and C9ORF72 fibroblasts. *Acta Neuropathol Commun* 2016;**4**:47.
30. Bardelli D, Sassone F, Colombrita C. *et al.* Reprogramming fibroblasts and peripheral blood cells from a *C9ORF72* patient: a proof-of-principle study. *J Cell Mol Med* 2020;**24**:4051–4060.
31. Santangelo S, Bossolasco P, Magri S. *et al.* Generation of an Ipsc line from a patient with spastic paraplegia type 10 carrying a novel mutation in KIF5A gene. *Stem Cell Res* 2023;**66**:103008.
32. Bossolasco P, Sassone F, Gumina V. *et al.* Motor neuron differentiation of iPSCs obtained from peripheral blood of a mutant TARDBP ALS patient. *Stem Cell Res* 2018;**30**:61–68.
33. Francia S, Cabrini M, Matti V. *et al.* DICER, DROSHA and DNA damage-response RNAs are necessary for the secondary recruitment of DNA damage response factors. *J Cell Sci* 2016;**129**: 1468–1476.
34. Ratti A, Peverelli S, D'Adda E. *et al.* Genetic and epigenetic disease modifiers in an Italian *C9orf72* family expressing ALS, FTD or PD clinical phenotypes. *Amyotroph Lateral Scler Frontotemporal Degener* 2022;**23**:292–298.
35. Ratti A, Gumina V, Lenzi P. *et al.* Chronic stress induces formation of stress granules and pathological TDP-43 aggregates in human ALS fibroblasts and iPSC-motoneurons. *Neurobiol Dis* 2020;**145**:105051.
36. Hansen JN, Rassmann S, Stüven B. *et al.* CiliaQ: a simple, open-source software for automated quantification of ciliary morphology and fluorescence in 2D, 3D, and 4D images. *EPGE* 2021;**44**:18.